Magnesium Technology 2011
Edited by: Wim H. Sillekens, Sean R. Agnew, Neale R. Neelameggham, and Suveen N. Mathaudhu
TMS (The Minerals, Metals & Materials Society), 2011

NANOCRYSTALLINE Mg-MATRIX COMPOSITES WITH ULTRAHIGH DAMPING PROPERTIES

Babak Anasori, Shahram Amini, Volker Presser and Michel W. Barsoum
Department of Materials Science and Engineering, Drexel University, Philadelphia, PA 19104, USA

Keywords: Mg-matrix composite, Nano composites, Liquid melt infiltration, Powder Metallurgy.

Abstract

Recently, we reported on the processing of 50 vol.% Ti_2AlC-nanocrystalline magnesium, nc-Mg, matrix composites using a pressureless melt infiltration method. Herein we report on composites with up to 80 vol.% Mg. These composites are readily machinable, relatively stiff, strong and light, and exhibit ultrahigh damping. Increasing the nc-Mg volume fraction leads to lighter composites with higher damping characteristics at lower stresses (~30% of the mechanical energy is dissipated at 250 MPa). In some cases the Mg nanograins are also extraordinarily thermally stable which renders these composites good candidates for applications at temperatures higher than ambient. Due to the simple inexpensive melt infiltration technique used to fabricate these novel nanocomposites, it is possible to produce samples as large as ones made via normal powder metallurgy methods.

Introduction

The MAX Phases

The $M_{n+1}AX_n$ (MAX) phases are layered hexagonal solids, with two formula units per unit cell, in which near close-packed layers of M are interleaved with layers of pure A-group elements, with the X-atoms filling the octahedral sites between the M layers. These solids combine some of the best attributes of metals and ceramics. Like metals, they are electrically and thermally conductive, most readily machinable [1, 2], not susceptible to thermal shock, plastic at high temperatures, and exceptionally damage tolerant [1-6]. Like ceramics, some of them are elastically rigid (Young's mod. > 300 GPa), lightweight (≈ 4 gm/cc) and maintain their strengths to high temperatures. The ternaries Ti_3SiC_2 and Ti_2AlC are creep, fatigue and oxidation resistant [7-10], which is one reason they were chosen for this work. The Ti-based MAX phases are also more conductive, both electrically and thermally than Ti metal at all temperatures [6, 11].

Due to their layered nature and the fact that basal slip is operative at all temperatures, the MAX phases possess unique mechanical properties that are atypical for structural ceramics. The fracture toughness of Ti_3SiC_2 exhibits R-curve behavior and varies from 8-16 $MPam^{1/2}$ depending on crack length [12, 13]. The latter value is one of the highest ever reported for a single-phase, monolithic ceramic. Such good damage tolerance is attributed in part to kinking and the formation of the heavily deformed lamellar bridges in the crack wake that are reminiscent of those that form in wood and other layered composites. The MAX phases also have excellent low and high-cycle fatigue properties [14]. For example, fine-grained Ti_3SiC_2 samples can be compressively loaded to 700 MPa for 100 cycles with no apparent fatigue [15, 16]. The reason for this state of affairs is believed to be the formation of fully reversible, dislocation-based incipient kink bands, IKBs, discussed in the next section. Note that in the MAX phases, every basal plane is a potential delamination and/or slip plane.

Kinking Nonlinear Elasticity

More recently it has been shown that the MAX phases are a subset of a much greater class of solids termed kinking nonlinear elastic, KNE, for which the only requirement for membership is plastic anisotropy, in the sense that dislocations are confined to two dimensions [15, 17, 18]. Plastic anisotropy insures that the formation of, non-basal dislocations is prohibitively expensive. These solids then deform by the formation of kink bands, KBs. Prior to the formation of the KBs, however, it has been shown that these solids must first form incipient kink bands, IKBs. IKBs are fully reversible dislocation-based loops that are nucleated on the easy slip planes of stressed, plastically anisotropic solids. IKBs are comprised of coaxial, parallel dislocation loops, with $2\alpha >> 2\beta$ (Fig. 1a) [15]. Frank and Stroh [19] showed that by virtue of their shape, IKBs, can only exist when a load is applied; removal of the load results in their shrinkage and ultimate annihilation and restores the perfect lattice. In recent papers, it was shown that IKBs are the precursors of mobile dislocation walls, MDWs, or low angle boundaries that, in turn, result in regular kink boundaries, KBs [20-22].

Using a Griffith-like approach, Frank and Stroh [19] showed that at a critical threshold stress, σ_t:

$$\tau_c \approx \frac{\sigma_t}{M} \approx \sqrt{\frac{G^2 b}{2\alpha\gamma_c}} \qquad (1)$$

a subcritical IKB becomes critical and would run to the ends of the two-dimensional crystal they modeled. In Eq. 1, M, G, b, and γ_c are, respectively, the Taylor factor, shear modulus, Burgers vector and the kinking angle, which is small and of the order of 3° or less. Based on our work to date it has been shown that 2α can be equated to grain dimension along [0001] [23]. Interestingly, this implies σ_t is proportional to $1/\sqrt{\text{grain size}}$, i.e. follows a Hall-Petch like relationship.

As noted above, removal of the stress restores the perfect crystal. The driving force for the collapse of the IKBs stems from their shape and is contingent on their ends remaining attached [21]. If the ends are sundered, the IKBs devolve into MDWs, also known as, low angle grain boundaries, which ultimately give rise to KBs; the latter are irreversible.

The signature of IKBs is the formation of fully reversible stress-strain loops [15, 22, 23] (Fig. 1b), whose size and shape are a strong function of grain size. Before discussing the relationship between IKBs, microyielding and damping in KNE solids, it is important to briefly summarize the major elements of the IKB-based model, which as noted above, is based on the aforementioned work by Frank and Stroh paper [19]. Referring to Fig. 1b:

i) a threshold stress, σ_t, given by Eq. 1, is needed to nucleate an IKB;

ii) the energy dissipated per unit volume per cycle, W_d, is given by [21, 23, 24]:

$$W_d = \frac{4\pi(1-\nu)N_k\alpha^3}{G^2\gamma_c M^2}\frac{\Omega}{b}(\sigma^2 - \sigma_t^2) \quad (2)$$

where N_k is the number of IKBs per unit volume, and Ω is the energy dissipated by a dislocation line sweeping a unit area. It follows that Ω/b is the critical resolved shear stress, CRSS, of the IKB dislocations. According to Eq. 2 W_d, scales with σ^2, with a x-axis intercept at σ_t^2 as observed (see below).

iii) Non-linear strain, ε_{NL} (defined in Fig. 1b). Recasting Eq. 2 in terms of ε_{NL} yields [21, 23, 24]:

$$W_d = 3k_1\frac{\Omega}{b}\varepsilon_{IKB} \quad (3)$$

It follows that Ω/b should be proportional, if not equal, to the CRSS of an IKB dislocation loop. k_1 relates the IKB volumetric strain to the axial strain along the loading direction. k_1 and typically is of the order of 1 or 2 depending on texture [25]. It follows that W_d should scale linearly with ε_{NL} as, repeatedly, observed. The slopes of such curves are directly proportional to the CRSS of the IKB dislocations [21, 22, 25]. In other words, using the IKB-based model the CRSS of the IKB dislocations can be extracted from compression of polycrystalline samples. For hexagonal metals, the values obtained are in good agreement with values measured in single crystal work [26].

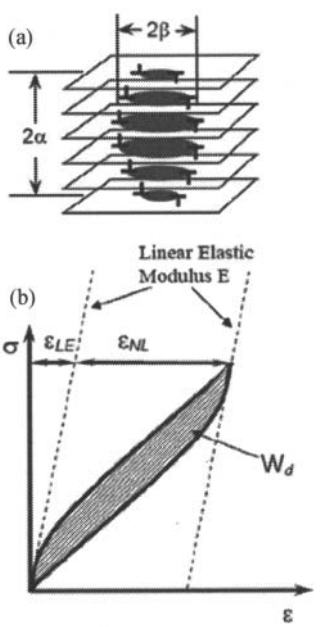

Figure 1. Schematic of (a) dislocation loops comprising an IKB, (b) typical stress-strain curve for a KNE solid and definitions of non-linear strain, ε_{NL} and energy dissipated per cycle, W_d.

With this insight we were not only able to explain our own results, but also the deformation of many diverse and seemingly unrelated solids such as graphite [27], the MAX phases [24, 28], sapphire [21], ZnO [22], $LiNbO_3$ [29], $LiTaO_3$ [30], mica [18, 31] and presumably other layered silicates and thus much of geology among many others.

Microyielding and Damping in Hexagonal Metals

The hexagonal close-packed metals, Ti, Mg, Co, Zr and Zn are of immense technological importance and have been studied extensively for the past 70 years. Despite this large amount of work, the nature of their damping and microyielding has remained unclear. Recently, we showed that when polycrystalline Co [23], Mg [20] or Ti [26], samples are loaded in simple compression fully reversible loops form above a threshold stress. The size and shape of these loops was found to be a strong function of grain size; large grained samples had significantly larger W_d values. The size of the loops, or W_d, was also a function of pre-strain. Increasing the deformation strain, reduces the domain or grain sizes, 2α, which increases σ_t which ultimately reduces W_d. Based on this IKB-based model it is possible to associate damping at stresses > σ_t in these solids with the to-and-fro motion of IKB dislocations. Results of this model, for example, explain why Mg and Zn are high damping metals, while Al is not.

Currently there is no direct evidence for the existence of IKBs. The circumstantial evidence for their existence, however, is compelling. Three dislocation-based possibilities for microyielding and damping exist: reversible dislocation pileups, reversible twinning and IKBs. For the former two, it can be shown that W_d should scale with σ, and not σ^2, as observed. The same physics also applies to solids in which twins form, such as Mg and Co, as to those that do not, such as the MAX phases. Lastly and most importantly, the CRSS values obtained from W_d vs. ε_{NL} plots are in good agreement with the same values measured from single crystal work [20, 22, 26].

Metal Matrix Composites Reinforced with MAX Phases

Based on the aforementioned ideas it was speculated that fabricating composites with two KNE solids should result in exceptionally high values of W_d. A natural choice was to combine Mg with commercially available MAX powders, such as Ti_3SiC_2 and Ti_2AlC. The results for Ti_2AlC-Mg composite were as unexpected as they were surprising in that the Mg matrix grains were at the nano-scale. The processing and microstructural characterization of 50 vol. % Ti_2AlC-nc Mg-matrix composites fabricated by pressureless spontaneous melt infiltration at 750 °C for 1 h can be found in Ref. [3]. X-ray diffraction and transmission electron microscopy, TEM, both confirmed that the Mg grain size was at nano scale [3].

The 50 vol.% Ti_2AlC/nc-Mg composites are readily machinable, stiff (effective E ≈ 70 GPa), strong, light (2.9 g/cm^3) and exhibited – at the time - record W_d values at σ levels of the order of ≈ 500 MPa. Since the IKB-based model predictions were well adhered to, it was concluded that the composite, like its individual components, was a KNE solid in which the nucleation and annihilation of IKBs was responsible for the high W_d values. The CRSS values extracted from the compression results were closer to those of Ti_2AlC than for Mg, indicating that it is the former than is responsible for the damping [32]. In other words, because it is at the nano-scale, the Mg does not form IKBs. The role of the Mg is to thus to impart strength to the composite and allow for high compressive stresses. In addition to their record damping – and presumably for the same reason, i.e. IKB formation – we have recently shown that the MAX/Mg composites are also quite fatigue resistant [33]. The aim of this work was to reduce the vol.

% of the reinforcement to 20 vol. % to obtain lighter samples with higher damping properties that would also be less expensive.

Experimental Details

In contrast to almost all the processes that used for the fabrication of nc metals, in general, and low melting point metals, like Mg, in particular, the method used here is quite simple and unique. The method has been used to fabricate Mg–50 vol. % Ti_2AlC by pressureless, spontaneous Mg melt-infiltration into a porous Ti_2AlC preforms [3]. In addition to this process, powder metallurgy was also used to make composites with higher volume fractions of Mg. The starting powders - Ti_2AlC (-325 mesh, 3-ONE-2, Voorhees, NJ) and Mg (-325 mesh, 99.8 % pure, Alfa Aesar, Ward Hill, MA) - were ball-milled for 12 h. Porous samples were fabricated from the powder mixtures in the form of rectangular bar (1.3 x 1.3 x 70 mm^3) by cold pressing at 50 MPa. Also for the sake of comparison, Mg-20 vol. % Ti_3SiC_2 composites were fabricated, using the same processing steps. In this case, the starting powders were Ti_3SiC_2 (- 325 mesh, 3-ONE-2, Voorhees, NJ), and the same Mg powder used above. The samples were placed in alumina, Al_2O_3, crucibles (AdValue Technology, Tucson, AZ) that were in turn covered with Al_2O_3 lids and placed in a graphite-heated vacuum-atmosphere hot press, (Series 3600, Centorr Vacuum Industries, Somerville, MA) heated at 10°C/min to 750°C, held at that temperature for 1 hour, after which the furnace was turned off and the samples were furnace cooled. The samples' microstructures were observed in a field emission scanning electron microscope, SEM, (Zeiss Supra 50VP, Germany). X-ray diffraction was carried out on a diffractometer (Model 500D, Siemens, Karlsruhe, Germany) and the spectra were collected using step scans of 0.01 in the range of 10°–80° 2 theta and a step time of 2 s. Scans were made with Cu Kα radiation (40 KV and 30 mA).

The room temperature compressive and cyclic uniaxial loading–unloading compression tests were measured using a hydraulic testing machine (MTS 810, Minneapolis, MN). The strains were measured by a capacitance extensometer (MTS, Minneapolis, MN) – attached to the samples – with a range of 1% strain. All the loading–unloading compression tests were performed in load-control mode at a loading rate of 54 MPa/s. The Vickers microhardness values, V_H, were measured using a microhardness indenter (LECO-M400, LECO Corp. St. Joseph, MI) at 10N.

Results and Discussion

Comparing the full width at half maximum, FWHM, of the various Mg peaks from the XRD diffractogram of the 20 vol. % Ti_2AlC composite with those of pure Mg powder ($d_{av} \approx 150$ μm), 50 vol. % Ti_2AlC and 50 vol. % Ti_3SiC_2, revealed that the Mg peaks broadening happened only when Ti_2AlC was used as the reinforcement (Fig. 2). Using the Scherrer formula [34] the particle size was estimated to be 90 ± 15 nm. Note that even by decreasing the volume fraction of Ti_2AlC to 20 vol. %, surprisingly, Mg grains are still at the nano scale.

The microstructure of a mounted, and polished, 20 vol. % Ti_2AlC sample (Fig. 3a) was quite homogeneous and apparently fully dense. The Ti_2AlC grain size was 20±10 μm. The fractured surface (Fig. 3b), however, showed the presence of nano Mg grains, some as fine as 35 nm, as well as sub-micron Mg single crystals (pointed to by arrows).

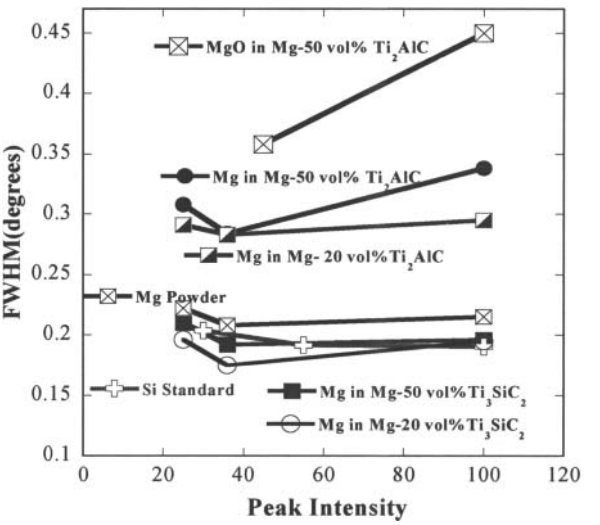

Figure 2. FWHM of Mg and MgO vs. peak intensity. The three highest intensity peaks in Mg and two in MgO are compared with those of a Si standard, pure as-received Mg powder peaks.

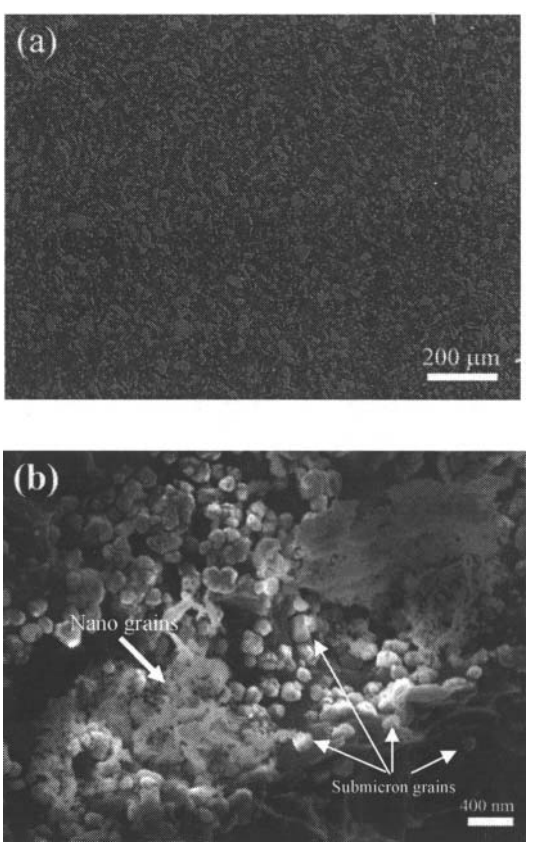

Figure 3. Secondary electron SEM images of, (a) polished surface of Mg-20 vol.% Ti_2AlC composite, (b) a fractured surface; arrows point to nano and sub-micron Mg grains.

Table I compares the microhardness values of the composites as a function of Ti_2AlC volume fractions and the hardness of a Mg- 30 vol. % SiC composite reported elsewhere [35]. The Vickers hardness of the composite with 20 vol. % Ti_2AlC is significantly higher than the composite with 30 vol. % of SiC confirming the nanoscopic nature of the Mg-grains.

Table I. Hardness of Mg-Ti_2AlC composites and Mg- 30 vol.% SiC composite

Material	Micro Hardness (GPa)
Mg- 50 vol.% Ti_2AlC	1.6±0.2
Mg- 20 vol.% Ti_2AlC	0.9±0.1
Mg- 30 vol.% SiC [35]	0.5

At 350±10 MPa, the ultimate compressive strength, UCS, of the 20 vol. % Ti_2AlC–Mg composite was lower than the 700±10 MPa of the 50 vol. % Ti_2AlC–Mg composites reported on earlier [3]. However, to confirm that the nanometer scale of the Mg-grains was mainly responsible for the high strengths observed we measured the UCS of Mg–50 vol.% Ti_3SiC_2 and Mg–20 vol.% Ti_3SiC_2 composites. In the latter two composites, as mentioned above, the Mg-grains were not in the nanometer scale and their UCSs, at 400±20 and 240±20 MPa, respectively, were lower than those of the Ti_2AlC–Mg composites with comparable volume fractions of reinforcement.

Typical compressive hysteretic stress–strain loops, at four different loads, up to 75% of the UCS, shifted horizontally for clarity, are shown in Fig. 4a. Based on these curves and the fact that W_d (Fig. 4b) and ε_{NL} both scale as σ^2 as predicted from IKB-based model are consistent with the fact that IKBs are responsible for both [15, 17, 18, 27, 36]. In other words, W_d and ε_{NL} are due to the formation and annihilation of IKBs. The value of W_d for the composite with 20 vol. % Ti_2AlC is ≈ 0.34 MJ/m^3 at 250 MPa. To the best of our knowledge, this value is the highest ever reported at 250 MPa. These materials can dissipate ≈ 30 % of the total mechanical energy applied during each cycle.

The effective Young's moduli – calculated from least squares fits of the entire data set and shown as diagonal lines bisecting the loops in Fig. 4a – range from 38 to 50 GPa. While there are many solids for which damping is higher (e.g., elastomers) we believe that the combination of W_d, compressive strengths and moduli values reported herein is unique and outside the Ashby envelope [37] (see intersection of dashed lines in Fig. 5). In the case of the composites the relatively softer Mg phase in between the Ti_2AlC grains allows the latter to kink. However, and in contradistinction to pores, that essentially achieve the same feat (for e.g. it was shown that a 10% porous Ti_2AlC sample had higher W_d values on an absolute scale than a fully dense one [28]) the presence of the nc-Mg allowed h much higher stress values to be reached before failure.

As noted above, W_d scales linearly with ε_{NL} with a slope that is equal to $3k_1$ Ω/b. Table II compares the calculated CRSSs of different materials tested. At 37 MPa, the Ω/b values obtained in the previous work [3], and for the 20 vol. % Ti_2AlC composites tested herein, are comparable to each other, and to those of bulk monolithic Ti_2AlC. This is important because it implies that most of the energy is dissipated in the Ti_2AlC phase. The decrease in Ω/b by increasing the volume fraction of Mg in the matrix can be

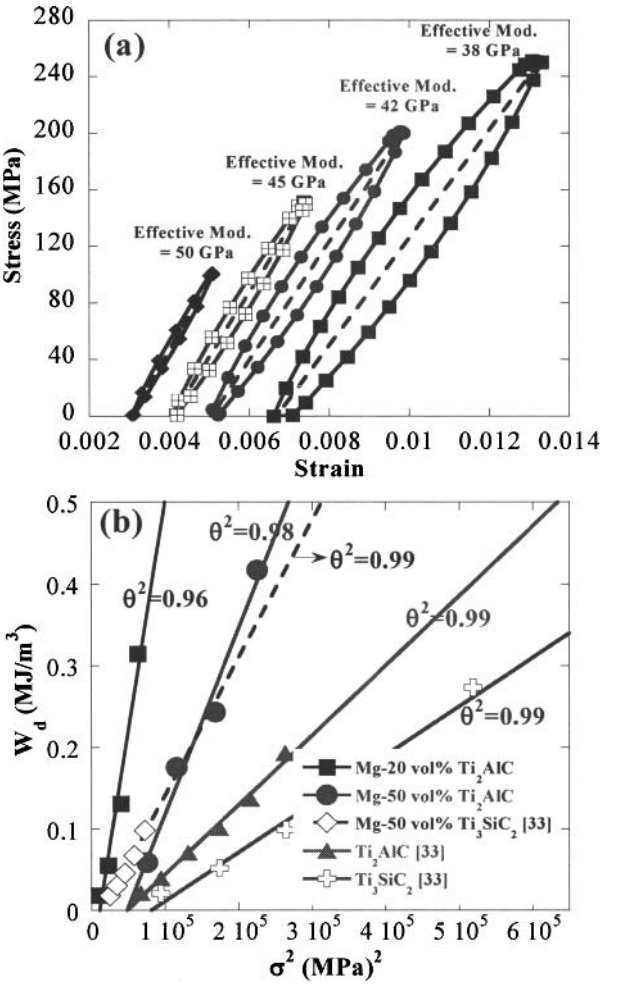

Figure 4. (a) Fully reversible hysteretic loops in a Mg-20 vol.% Ti_2AlC composite. The sample was compressed to ~ 75% of its failure stress; the loops are shifted horizontally for clarity; (b) Plot of W_d vs. σ^2 obtained from the uniaxial compression stress–strain curves.

Table II. Calculated Ω/b values from Eq. (3)

Material	$3k_1\Omega/b$	Ω/b (MPa)
Ti_2AlC [32]	228	38
Mg-50 vol% Ti_2AlC	233	37
Mg-20 vol% Ti_2AlC	200	33
Ti_3SiC_2 [32]	192	32
Mg-50 vol% Ti_3SiC_2 [32]	93	15.5
Mg [26]	24	4

related to the grain size of the Mg; by having larger Mg grains the possibility of forming IKBs in the latter increases. As noted above, the fact that a 10% porous Ti_2AlC sample dissipates more energy per unit volume per cycle on an absolute scale than its fully dense counterpart [28] essentially eliminates all mechanisms,

such as dislocation pileups and/or twinning that scale directly with the volume of the material tested. It is, however, in agreement with an IKB-based model in which kinking – which is a form of plastic instability, or buckling - is more prone to happen in a less rigid or porous solid than a fully dense one.

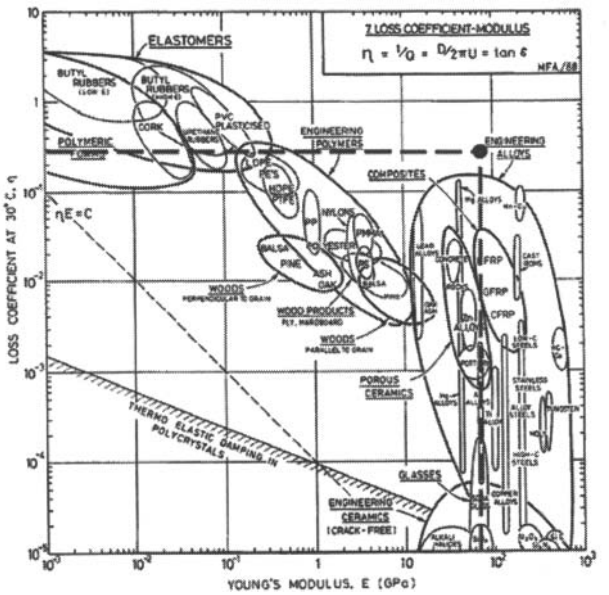

Figure 5. Ashby map of log of loss coefficients vs. log of Young's moduli [37]. The intersection of the two dotted lines is where some of our composites fall; clearly outside the envelope.

In contrast to the aforementioned case where the Ti_2AlC phase is responsible for most of the energy dissipated per cycle, the situation for the Mg-Ti_3SiC_2 composites is substantially different. At 16 MPa, the Ω/b value appears to be an average of that of Ti_3SiC_2 (32 MPa) and Mg (4 MPa). This suggests that in this case, both the Mg and Ti_3SiC_2 contribute to Ω/b, and hence W_d [32].

Accompanying the record strengths and damping is a nc-Mg matrix that is remarkably stable [38]. The microstructure is so stable that heating the composite three times to 700 °C – 50 °C over the melting point of Mg – not only resulted in the repeated melting of the Mg, but surprisingly and within the resolution of our differential scanning calorimeter did not lead to any coarsening (Fig. 6). The reduction in the Mg melting point due to the nano-grains in the 20 vol.% Ti_2AlC composite was ≈ 20 °C which is less than the 50 °C reported for the Mg- 50 vol.% Ti_2AlC [38]. This is most probably because the Mg nano-grains in the latter are smaller than the former. For the Mg-50 vol. % Ti_2AlC composites, XRD and neutron diffraction results suggested that a thin, amorphous and/or poorly crystallized rutile/anatase/magnesia layer separate the Mg nanograins and prevent them from coarsening [38]. That layer is presumably thin enough and thus mechanically robust enough to survive the melting and solidification stresses encountered during thermal cycling.

Summary and Concluding Remarks

Stiffness, in general, and high specific stiffness in particular are desirable qualities in solids. Typically, the price paid for high stiffness is lack of damping (Fig. 5). High specific stiffness exacts another price: difficulty in machinability, which can add considerable complexity, weight and cost to components and structures. From a design point of view it would be advantageous if multi-functionality could be engineered into alloys or composites, such that the same load-bearing material could also dampen vibrations or noise while remaining easily machinable and stiff. The Mg-Ti_2AlC composites fabricated here are readily machinable, with strengths that range from 350 to 700 MPa in compression, stiffness values that range from 40 to 70 GPa, a density of 2 to 2.9 Mg/m^3, that can also dissipate ≈ 30% of the mechanical energy during each cycle.

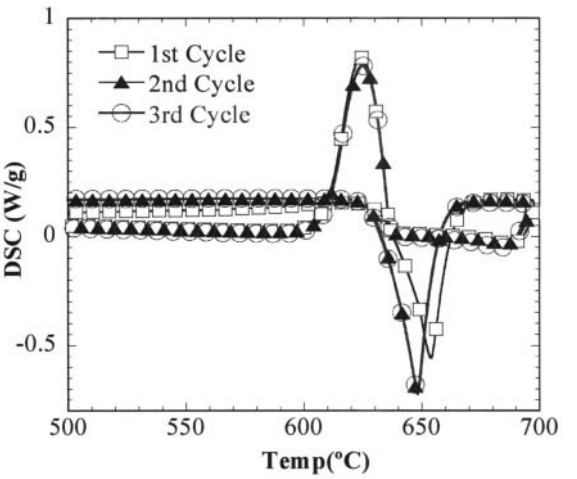

Figure 6. Three consecutive DSC cycles from 100°C to 700 °C of Mg- 20 vol. % Ti_2AlC composite.

More recently, much emphasis has been given to nano scaled solids for structural applications and while the advantages of nanostructured solids in some applications are clear, making the latter economically and on an industrial scale has been more of a challenge. The techniques used here - either simple spontaneous melt infiltration of Mg into porous ceramics preforms or powder metallurgy processes - are simple and inexpensive. Note that since the wetting and subsequent infiltration are spontaneous, there should be, in principle, no limits to the sizes or shapes of the samples, which in turn would allow for the production of large, net-, or near net-shape parts or components.

In addition to the simple fabrication techniques, the Mg nano grains, in contrast to other nano-grained solids, are extraordinary thermally stable which make them potentially good candidates for application at temperatures higher than ambient.

Acknowledgement

This work was supported by the Army Research Office (No. W911NF-07-1-0628).

References

1. Barsoum MW, Brodkin D, ElRaghy T. "Layered machinable ceramics for high temperature applications," *Scripta Materialia*, 36 (1997), 535-541.
2. Barsoum MW, ElRaghy T. "Synthesis and characterization of a remarkable ceramic: Ti3SiC2," *Journal of the American Ceramic Society*, 79 (1996), 1953-1956.

3. Amini S, Ni CY, Barsoum MW. "Processing, microstructural characterization and mechanical properties of a Ti2AlC/nanocrystalline Mg-matrix composite," *Composites Science and Technology*, 69 (2009), 414-420.
4. Barsoum MW, El-Raghy T. "Room-temperature ductile carbides," *Metallurgical and Materials Transactions a-Physical Metallurgy and Materials Science*, 30 (1999), 363-369.
5. Barsoum MW, El-Raghy T, Rawn CJ, Porter WD, Wang H, Payzant EA, Hubbard CR. "Thermal properties of Ti3SiC2," *Journal of Physics and Chemistry of Solids*, 60 (1999), 429-439.
6. Barsoum MW, Flemings MC, Kramer EJ, Mahajan S, Veyssiere P. "Physical properties of the MAX phases," *In: Encyclopedia of materials science and technology*, (2006).
7. Amini S, McGhie AR, Barsoum MW. "Isothermal Oxidation of Ti2SC in Air," *Journal of the Electrochemical Society*, 156 (2009), P101-P106.
8. Barsoum MW, Ho-Duc LH, Radovic M, El-Raghy T. "Long time oxidation study of Ti3SiC2,Ti3SiC2/SiC, and Ti3SiC2/TiC composites in air," *Journal of the Electrochemical Society*, 150 (2003), B166-B175.
9. Barsoum MW, ElRaghy T, Ogbuji LUJT. "Oxidation of Ti3SiC2 in air," *Journal of the Electrochemical Society*, 144 (1997), 2508-2516.
10. Low IM, Lee SK, Lawn BR, Barsoum MW. "Contact damage accumulation in Ti3SiC2," *Journal of the American Ceramic Society*, 81 (1998), 225-228.
11. Barsoum MW, Yoo HI, Polushina IK, Rud VY, Rud YV, El-Raghy T. "Electrical conductivity, thermopower, and hall effect of Ti_3AlC_2, Ti_4AlN_3, and Ti_3SiC_2," *Physical Review B*, 62 (2000), 10194-10198.
12. Chen D, Shirato K, Barsoum MW, El-Raghy T, Ritchie RO. "Cyclic fatigue-crack growth and fracture properties in Ti3SiC2 ceramics at elevated temperatures," *Journal of the American Ceramic Society*, 84 (2001), 2914-2920.
13. Gilbert CJ, Bloyer DR, Barsoum MW, El-Raghy T, Tomsia AP, Ritchie RO. "Fatigue-crack growth and fracture properties of coarse and fine-grained Ti3SiC2," *Scripta Materialia*, 42 (2000), 761-767.
14. Zhang H, Wang ZG, Zang QS, Zhang ZF, Sun ZM. "Cyclic fatigue crack propagation behavior of Ti3SiC2 synthesized by pulse discharge sintering (PDS) technique," *Scripta Materialia*, 49 (2003), 87-92.
15. Barsoum MW, Zhen T, Kalidindi SR, Radovic M, Murugaiah A. "Fully reversible, dislocation-based compressive deformation of Ti3SiC2 to 1GPa," *Nature Materials*, 2 (2003), 107-111.
16. Zhen T, Barsoum MW, Kalidindi SR. "Effects of temperature, strain rate and grain size on the compressive properties of Ti3SiC2," *Acta Materialia*, 53 (2005), 4163-4171.
17. Barsoum MW, Zhen T, Zhou A, Basu S, Kalidindi SR. "Microscale modeling of kinking nonlinear elastic solids," *Physical Review B*, 71 (2005), 134101.
18. Barsoum MW, Murugaiah A, Kalidindi SR, Zhen T. "Kinking nonlinear elastic solids, nanoindentations, and geology," *Physical Review Letters*, 92 (2004), -.
19. Frank FC, Stroh AN. "On the Theory of Kinking," *Proceedings of the Physical Society*, **65** (1952), 811-821
20. Zhou AG, Barsoum MW. "Kinking Nonlinear Elasticity and the Deformation of Magnesium," *Metallurgical and Materials Transactions a-Physical Metallurgy and Materials Science*, 40A (2009), 1741-1756.
21. Basu S, Barsoum MW, Kalidindi SR. "Sapphire: A kinking nonlinear elastic solid," *Journal of Applied Physics*, 99 (2006).
22. Basu S, Barsoum MW. "Deformation micromechanisms of ZnO single crystals as determined from spherical nanoindentation stress-strain curves," *Journal of Materials Research*, 22 (2007), 2470-2477.
23. Zhou AG, Brown D, Vogel S, Yeheskel O, Barsoum MW. "On the kinking nonlinear elastic deformation of cobalt," *Materials Science and Engineering A*, 527 (2010), 4664-4673.
24. Amini S, Zhou A, Gupta S, DeVillier A, Finkel P, Barsoum MW. "Synthesis and elastic and mechanical properties of Cr2GeC," *Journal of Materials Research*, 23 (2008), 2157-2165.
25. Reed-Hill RE, Dahlberg EP, Slippy WA, Jr., "Some anelastic effects in zirconium at room temperature resulting from prestrain at 77K," *Transactions of the Metallurgical Society of AIME*, 233 (1965), 1766-1771.
26. Zhou AG, Basu S, Barsoum MW. "Kinking Nonlinear Elasticity, Damping and Microyielding of Hexagonal Closed-Packed Metals," *Acta Materialia*, 59 (2008), 60-67.
27. Barsoum MW, Murugaiah A, Kalidindi SR, Zhen T, Gogotsi Y. "Kink bands, nonlinear elasticity and nanoindentations in graphite," *Carbon*, 42 (2004), 1435-1445.
28. Zhou AG, Barsoum MW, Basu S, Kalidindi SR, El-Raghy T. "Incipient and regular kink bands in fully dense and 10 vol.% porous Ti2AlC," *Acta Materialia*, 54 (2006), 1631-1639.
29. Basu S, Zhou AG, Barsoum MW. "Reversible dislocation motion under contact loading in LiNbO3 single crystal," *Journal of Materials Research*, 23 (2008), 1334-1338.
30. Anasori B, Sickafus KE, Usov IO, Barsoum MW. "Spherical Nanoindentation Study, and Effects of Ion Irradiation on the Deformation Micromechanisms of LiTaO3 Single Crystals," *Sub. for pub.*, (2010).
31. Basu S, Zhou A, Barsoum MW. "On spherical nanoindentations, kinking nonlinear elasticity of mica single crystals and their geological implications," *Journal of Structural Geology*, 31 (2009), 791-801.
32. Amini S, Barsoum MW. "On the effect of texture on the mechanical and damping properties of nanocrystalline Mg-matrix composites reinforced with MAX phases," *Materials Science and Engineering a-Structural Materials Properties Microstructure and Processing*, 527 (2010), 3707-3718.
33. Kontsos A, Hazeli K, Anasori B, Loutas T, Sotiriadis G, Kostopoulos V, Barsoum MW. Grain Size Effect on the Fatigue Response of Nanocrystalline Magnesium Composites Reinforced with MAX Phases. 9th HSTAM International Congress on Mechanics. Limassol, Cyprus, (2010).
34. Scherrer P. "Bestimmung der Größe und der inneren Struktur von Kolloidteilchen mittels Röntgenstrahlen," *Nachrichten von der Gesellschaft der Wissenschaften zu Göttingen*, 2 (1918), 98-100.
35. Saravanan RA, Surappa MK. "Fabrication and characterisation of pure magnesium-30 vol.% SiCP particle composite," *Materials Science and Engineering a-Structural Materials Properties Microstructure and Processing*, 276 (2000), 108-116.
36. Barsoum MW, Radovic M, Zhen T, Finkel P, Kalidindi SR. "Dynamic elastic hysteretic solids and dislocations," *Physical Review Letters*, 94 (2005), -.
37. Ashby MF. "On the Engineering Properties of Materials," *Acta Metallurgica*, 37 (1989), 1273-1293.
38. Amini S, Cordoba JM, Daemen L, McGhie AR, Ni CY, Hultman L, Oden M, Barsoum MW. "On the Stability of Mg Nanograins to Coarsening after Repeated Melting," *Nano Letters*, 9 (2009), 3082-3086.